Appendix A. Supporting information

Resolving CO_2 activation and hydrogenation pathways over iron carbides from DFT investigation

Xianglin Liu[a], Chenxi Cao[a], Pengfei Tian[a], Minghui Zhu[a], Yulong Zhang[a], Jing Xu[a,*], Yun Tian[b], Yi-Fan Han[a,b,*]

[a] State Key Laboratory of Chemical Engineering, East China University of Science and Technology, Shanghai 200237, China

[b] Engineering Research Center of Advanced Functional Material Manufacturing of Ministry of Education, Zhengzhou University, Zhengzhou 450001, China

* Corresponding author phone: (+86) 021-64251938; fax: (+86) 021-64251938

E-mail: yifanhan@ecust.edu.cn; xujing@ecust.edu.cn

Method

In this work, periodic spin-polarized density functional theory (DFT) calculations were performed using the Vienna ab initio simulation package (VASP) [1-4]. The projected augmented wave (PAW)[5] pseudopotentials were used to describe the interactions between valence and core electrons. The exchange correlation energy of the electrons was treated with the Perdew, Burke, and Ernzerhof (PBE)[6] functional within the generalized gradient approximation (GGA) [7]. The solution of the Kohn−Sham equations was expanded in a plane wave basis set with a cutoff energy of 400 eV, and the sampling of the Brillouin zone was performed using the Monkhorst−Pack scheme [8,9]. Electron smearing was employed via the Methfessel−Paxton technique with a smearing width consistent to 0.2 eV. The TS were searched by combining the climbing image nudged elastic band (CI-NEB) method [10] with the dimer method [11]. The dimer separation was set to 0.01 Å, and the force convergence on each atom was less than 0.05 eV/Å. All vibrational analysis for the adsorbates and transition states were calculated to confirm the reliability of the calculated values (Table S13-S20). Bader charge analysis and charge density difference analysis were performed using the code developed by Henkelman and co-workers [12,13].

The surface energy (E_{surf}) was determined by equation (Eq) 1:

$$E_{surf} = (E_{slab} - N \times E_{bulk}) / 2\mathrm{A} \qquad \text{.....} (1)$$

where E_{slab} and E_{bulk} are the total energies of the supercell slab and one bulk unit cell, respectively, N is the number of bulk units in the slab, and A is the surface area of the slab.

The adsorption energy (E_{ads}) was defined as Eq2:

$$E_{ads} = E_{(adsorbates + slab)} - \left(E_{slab} + E_{adsorbates}\right) \quad \text{……………………... (2)}$$

where $E_{(adsorbates + slab)}$ is the total energy of the slab with adsorbates, E_{slab} is the total energy of the corresponding bare slab, and $E_{adsorbates}$ is the total energy of free adsorbates. Hence, a negative (positive) value indicates an exothermic (endothermic) adsorption. In principle, the more negative the E_{ads}, the stronger the binding.

The reaction energy (E_r) and barrier (E_a) were calculated by Eq3 and 4:

$$E_r = E_{FS} - E_{IS} \quad \text{…………………………………………... (3)}$$

$$E_a = E_{TS} - E_{IS} \quad \text{…………………………………………... (4)}$$

where E_{IS}, E_{TS} and E_{FS} are the total energy of the corresponding initial state (IS), IS state (TS) and final state (FS), respectively.

The d-band center (ε_d) was used to correlate the catalytic properties with the electronic structure of the catalyst. It was calculated using Eq5:

$$\varepsilon_d = \frac{\int_{-\infty}^{+\infty} \rho_d(E) E dE}{\int_{-\infty}^{+\infty} \rho_d(E) dE} \quad \text{…………………………………………... (5)}$$

where E is the energy with respect to the Fermi energy, and $\rho_d(E)$ is the density of states projected onto the metal atom’s d-band at energy E.

Model

Bulk χ-Fe_5C_2 (Fig. 1(a)) is a monoclinic crystal and shows a C2/c crystallographic symmetry including 20 Fe and 8 C atoms per unit cell. Bulk θ-Fe_3C (Fig. 1(b)) is an orthorhombic crystal and exhibits a Pnma crystallographic symmetry containing 12 Fe and 4 C atoms per unit cell. The bulk structure of χ-Fe_5C_2 (θ-Fe_3C) was optimized with a 3 × 5 × 5 (9 × 7 × 9) Monkhorst–Pack k-point mesh. The optimized lattice parameters were in good agreement with previous experimental and theoretical values, as shown in Table S1.

Results

Surface energies of typical low Miller index facets and the specific high Miller index facets were calculated as shown in Table S2. The surface energies of the high Miller index (510) facet for χ-Fe_5C_2 (510) and (031) for θ-Fe_3C are the lowest among the calculated ones, indicating that χ-Fe_5C_2 (510) and θ-Fe_3C (031) are the most thermodynamically stable facets. This is consistent with previous experimental and theoretical results [14,15]. Thus, in this work, the supercell of p (1 × 1) for χ-Fe_5C_2 (510) surface including 8 layers of carbon and 20 layers of iron and a p (1 × 1) for θ-Fe_3C (031) slab with 4 layers of carbon and 12 layers of iron were constructed to represent the iron carbide catalysts. A vacuum gap spacing of 10.5 Å was used to avoid interaction between the repeating slabs. The validity of slab models had been verified (Table S4, S5 and S6).

For the χ-Fe_5C_2 (510) model, the bottom 11 Fe layers and 5 C layers (11Fe + 5C) were fixed at their bulk positions, while the top 12 layers (9Fe + 3C) and adsorbates were allowed to relax. As for θ-Fe_3C (031) slab, the top 7 layers (6Fe + 1C) and adsorbates were allowed to relax, while the bottom 9 layers (6Fe + 3C) were constrained at the bulk positions. A k-space mesh of 3 × 1 × 1 within the Monkhorst−Pack scheme was used to sample the Brillouin zone of the surface. The test of Monkhorst−Pack meshes is given in Table S7. For isolated molecules and atoms, calculations were carried out in a 10 Å × 10 Å × 10 Å box with a 1 × 1 × 1 Monkhorst-Pack k-point mesh. Spin-polarized calculations were performed considering the ferromagnetic nature of Fe.

In addition, charge analysis of surface atoms was performed to predict and interpret the adsorption position of reactants (Fig. S1). The iron atoms within the flat trapezoid-type and the ridge-type sites exhibit strong electron transport capabilities, thus could be effective sites for CO_2 adsorption and activation. These potential active sites are abundant on both χ-Fe_5C_2 (510) and θ-Fe_3C (031) surfaces, suggesting the comparability and reactivity of two surfaces. The surface site represents the position of CO_2 before optimization. For instance, $3F^1$ represents the first 3-fold hollow site; $4F^1$ represents the first 4-fold hollow site; Cs^1 represents the first surface carbon site; Fe^1 represents the surface iron atom site.

We first examined CO_2 adsorption on χ-Fe_5C_2 (510) and θ-Fe_3C (031), which are identified as the active phases of Fe-based catalysts. Starting from the energetically stable adsorption configurations, CO_2 activation pathways were subsequently investigated to elucidate the mechanism of CO_2 hydrogenation over the two iron carbides.

On χ-Fe_5C_2 (510) facet, CO_2 adsorption at the $3F^5$ site is the most stable (Fig. S2(b)). The C atom resides on the bridge between Fe^5 and Fe^6; the O^1 and O^2 of CO_2 form O-Fe bonds with Fe^6 and Fe^5, respectively. The bond lengths of C-O^1 and C-O^2 are both 1.25 Å, with an O-C-O bond angle of 138.8° (For gas phase CO_2 in comparison, the C-O bond lengths are 1.18 Å and the O-C-O bond angle is 180.0°), indicating initial activation of CO_2 upon adsorption.

On θ-Fe_3C (031) facet, CO_2 adsorption at the $3F^4$ site is the most stable (Fig. S6(b)). The C atom is on the top of Fe^5, while the O^2 of CO_2 bonds with Fe^4 and Fe^6 on the bridge site, and O^1 on the top of Fe^5. The bond lengths of C-O^1 and C-O^2 in the adsorbed-state CO_2 are elongated to 1.23 Å and 1.33 Å, respectively. The O-C-O bond angle bends to 130.8° in the adsorbed state. Configurations of the adsorbed state CO_2 enormously deviates from molecular CO_2 in the gas phase, suggesting initial activation of the molecule upon adsorption.

As for CO_2 direct dissociation over χ-Fe_5C_2 (510) surface, the easiest is at $3F^4$ site with CO_2 adsorption of -0.52 eV (Fig. 2(a)). In the TS, the bond length of C and O^2 elongated to 1.66 Å. C in CO_2 migrates to the top of Fe^6 and O^2 is located at the bridge site between Fe^3 and Fe^5. In addition, the O-C-O angle bends from 131.1° to 115.1° in the TS. Whereas, CO_2 direct dissociation θ-Fe_3C (031) facets at the $3F^3$ site is most favorable with CO_2 adsorption energy of -0.58 eV (Fig. 2(b)). In the TS, the angle of O-C-O reduces to 114.9° and the C–O^2 bond length elongated to 1.68 Å from 1.34 Å in the IS. The C dissociated from *CO_2 transfers to the Fe^5 top site with a C-Fe bond length of 1.90 Å with O^1.

CO_2 activation can undergo hydrogen assisted pathway except for the direct dissociation. The stability of *HCOO *COOH and *CO and *OH intermediates on χ-Fe_5C_2 (510) facet were verified as the first FS and the second IS. And to compare inclination of activation pathway with CO_2 direct dissociation, the C-O bond breakage with H assistance was taken into consideration. It is found that the activation energy barrier is mainly focus on the first TS.

In the TS of *CO and *OH in one step pathway on χ-Fe_5C_2 (510) facet (Fig. 3(a)), C-O^2 bond is elongated to 1.73 Å accompanied by C adatom from Fe^3 and Fe^5 bridge site migrates to Fe^4. In the final state, the H adatom transfers to Fe^5 and Fe^6 bridge site and then combines with O^2 with a bond length of 0.98 Å, additionally, *CO^1 settles in inclined top of Fe^3.

For the *COOH intermediate pathway on χ-Fe_5C_2 (510) facet (Fig. 3(b)), in the first transition state (TS1), adsorbed H transfers towards O of *CO_2 and the distance between them reduces to 1.45 Å from 2.67 Å in the IS. The formed *COOH configuration is mono-dentate. The *COOH intermediate then disintegrates into *CO and *OH with an energy barrier of 0.34 eV. In the second transition state (TS2), the C-O^2 bond length of *CO_2 is enlarged to 1.35 Å from 1.34 Å, and the O-C-O angle increases to 112.9° from 111.4°. In the second final state (FS2), *CO^1 is adsorbed at $4F^1$

site and the *O^2H migrates to 3F^2 site.

For the *HCOO intermediate pathway on χ-Fe_5C_2 (510) facet (Fig. 3(c)), in TS1, adsorbed H transfers towards C of *CO_2 and the distance between them reduces to 1.69 Å from 2.90 Å in the IS. The O-C-O angle decreases to 126.1° from 131.8°. In addition, the *CO_2 configuration becomes bi-dentate from mono-dentate in the IS. The formed *HCOO intermediate then disintegrates into *HCO and *O with an energy barrier of 0.57 eV. In the TS2, O^2 of *CO_2 transfers to the bridge site between Fe^4 and Fe^6 from the bridge site between Fe^3 and Fe^6 and the distance is enlarged to 2.81 Å between C and O^2. C migrates to the bridge site between Fe^6 and Fe^8 from Fe^6 top site. In the FS2, O^2 is adsorbed at 4F^1 site and C transfers to the bridge site between Fe^5 and Fe^8.

For the *COOH intermediate pathway on θ-Fe_3C (031) facet (Fig. 4(b)), in TS1, adsorbed H transfers towards O^2 of *CO_2 and the distance between them reduces to 1.49 Å from 2.73 Å in the IS. The *COOH configuration is mono-dentate. The *COOH intermediate then disintegrates into *CO and *OH with an energy barrier of 0.56 eV. In the TS2, the distance between O^2 and C is enlarged to 1.37 Å from 1.34 Å and the O-C-O angle increases to 114.7° from 111.6°. In the FS2, *CO^1 migrates to the top site of Fe^5, *O^2H transfers to the bridge site between Fe^6 and Fe^8.

In the TS of *CO and *OH in one step pathway on θ-Fe_3C (0 31) facet (Fig. 4(a)), adsorbed H transfers towards O^2 of *CO_2 and the distance is shortened to 1.41 Å from 2.58 Å in the IS. C of *CO_2 moves to Fe^3 accompanied by O^1 and the C-O^2 bond length is stretched to 2.94 Å, indicating the completely broken C-O bond. In FS,

*O^2H is adsorbed at bridge site between Fe^4 and Fe^6 and *CO^1 is trapped at $3F^3$ site.

As for *HCOO intermediate pathway on θ-Fe_3C (031) facet (Fig. 4(c)), in the first transition state (TS1), adsorbed H transfers towards C of *CO_2 and the distance between them reduces to 1.42 Å from 2.02 Å in the IS. And then formed *HCOO intermediate disintegrates into *HCO and *O with an energy barrier of 0.1 eV. In the second transition state (TS2), O^1 of *CO_2 transfers from Fe^3 to bridge site between Fe^3 and Fe^4; O^2 migrates to $4F^1$ site from the bridge site between Fe^4 and Fe^6. The C-O^2 bond length is enlarged from 1.36 Å to 2.74 Å.

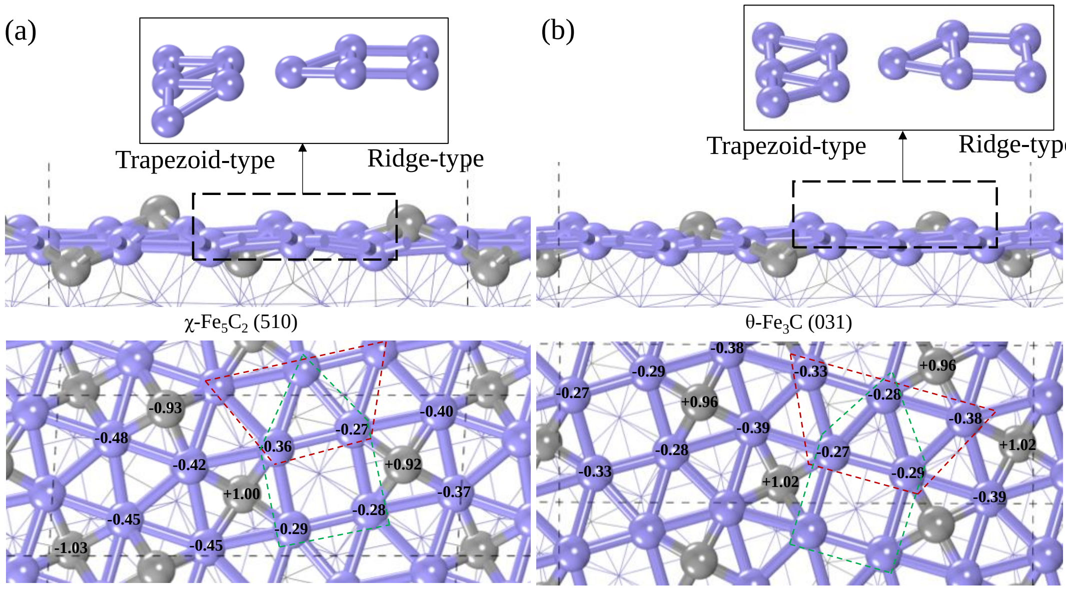

Fig. S1. Charge analysis for surface atoms of (a) χ-Fe_5C_2 (510) and (b) θ-Fe_3C (031). (Fe atoms in purple; C atoms in gray.)

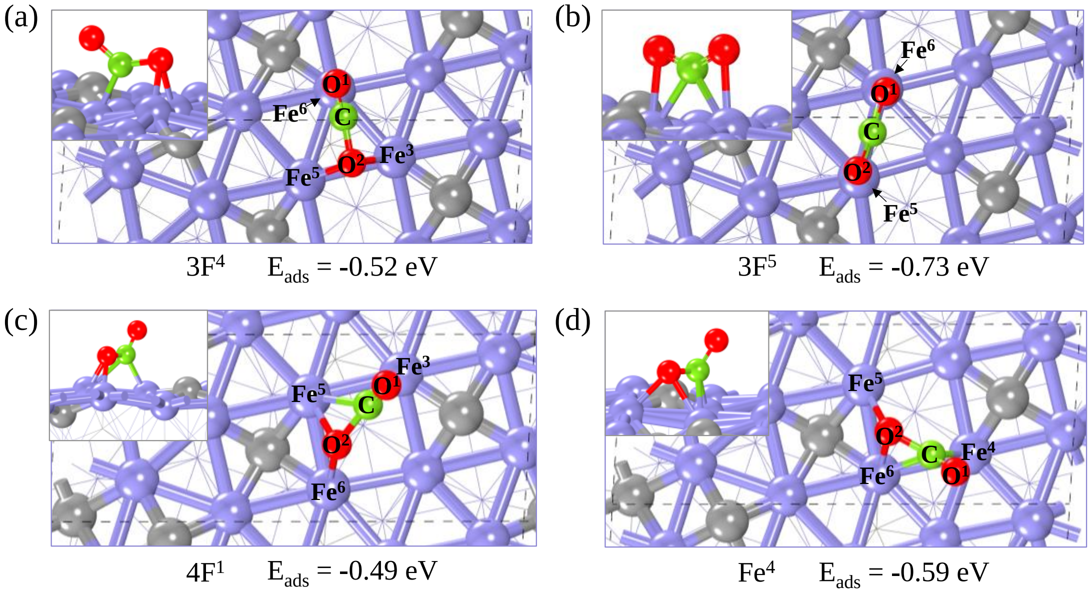

Fig. S2. Stable CO_2 adsorption configurations and the corresponding adsorption energies on χ-Fe_5C_2 (510) surface. (Fe atoms in purple, C atoms of χ-Fe_5C_2 in gray, C atoms of CO_2 in green, O atoms of CO_2 in red.)

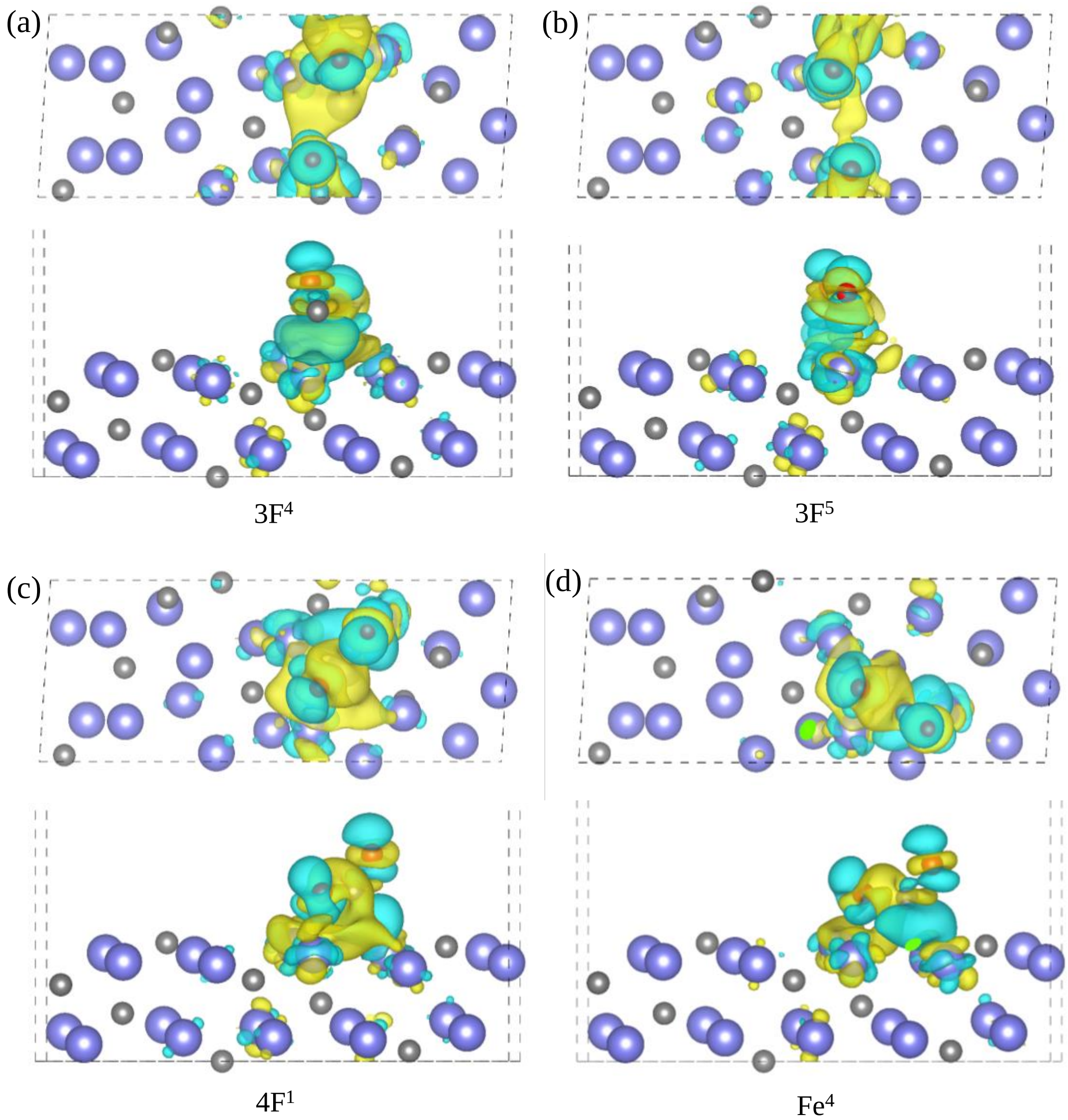

Fig. S3. Top and side views of charge densities for stable CO_2 adsorption structure on χ-Fe_5C_2 (510). (Fe atoms in purple; O atoms in red; C atoms in gray.) Yellow and cyan isosurfaces represent the charge accumulation (i.e. a gain of electron density) and depletion (i.e. a loss of electron density) in the system, respectively.

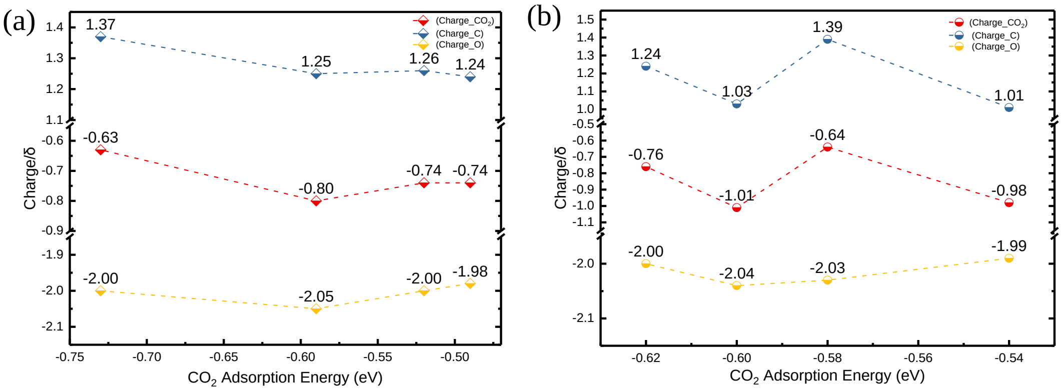

Fig. S4. The relationship between the stable adsorption energies and the number of electrons transferred over (a) χ-Fe_5C_2 (510) and (b) θ-Fe_3C (031) surfaces.

(a) (b)

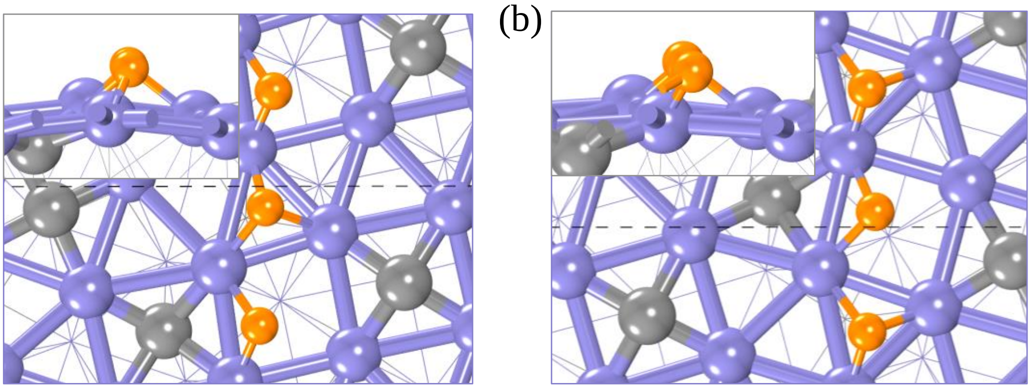

χ-Fe_5C_2 (510) E_{ads} = -1.33 eV θ-Fe_3C (031) E_{ads} = -1.32 eV

Fig. S5. Optimized structures of H_2 adsorption and dissociation on (a) χ-Fe_5C_2 (510) and (b) θ-Fe_3C (031) surfaces. (Fe atoms in purple; O atoms in red; H atoms in orange.)

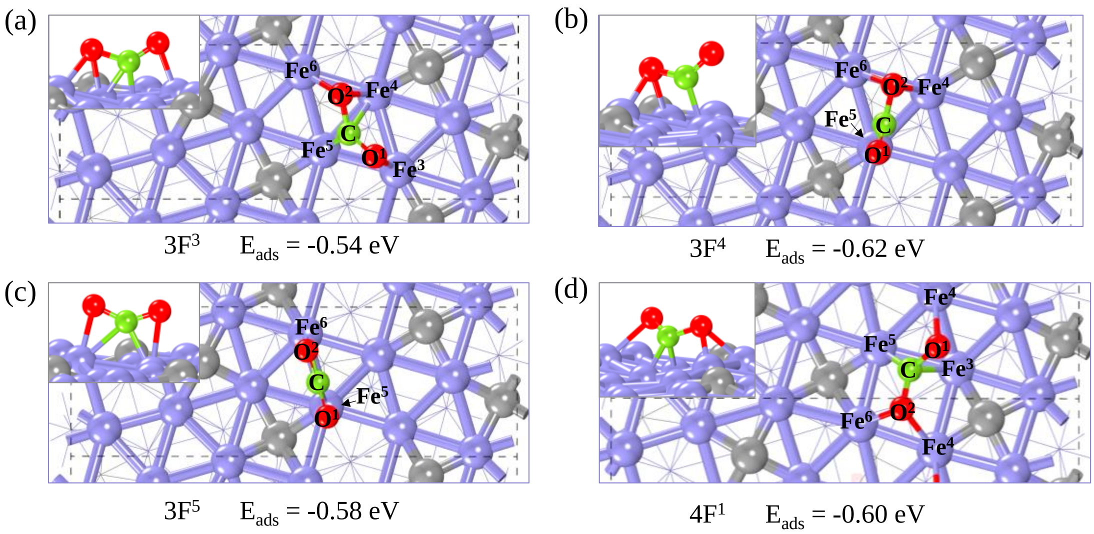

Fig. S6. Stable CO_2 adsorption configurations and the corresponding adsorption energies on θ-Fe_3C (031) surface. (Fe atoms in purple, C atoms of θ-Fe_3C (031) in gray, C atoms of CO_2 in green, O atoms of CO_2 in red.)

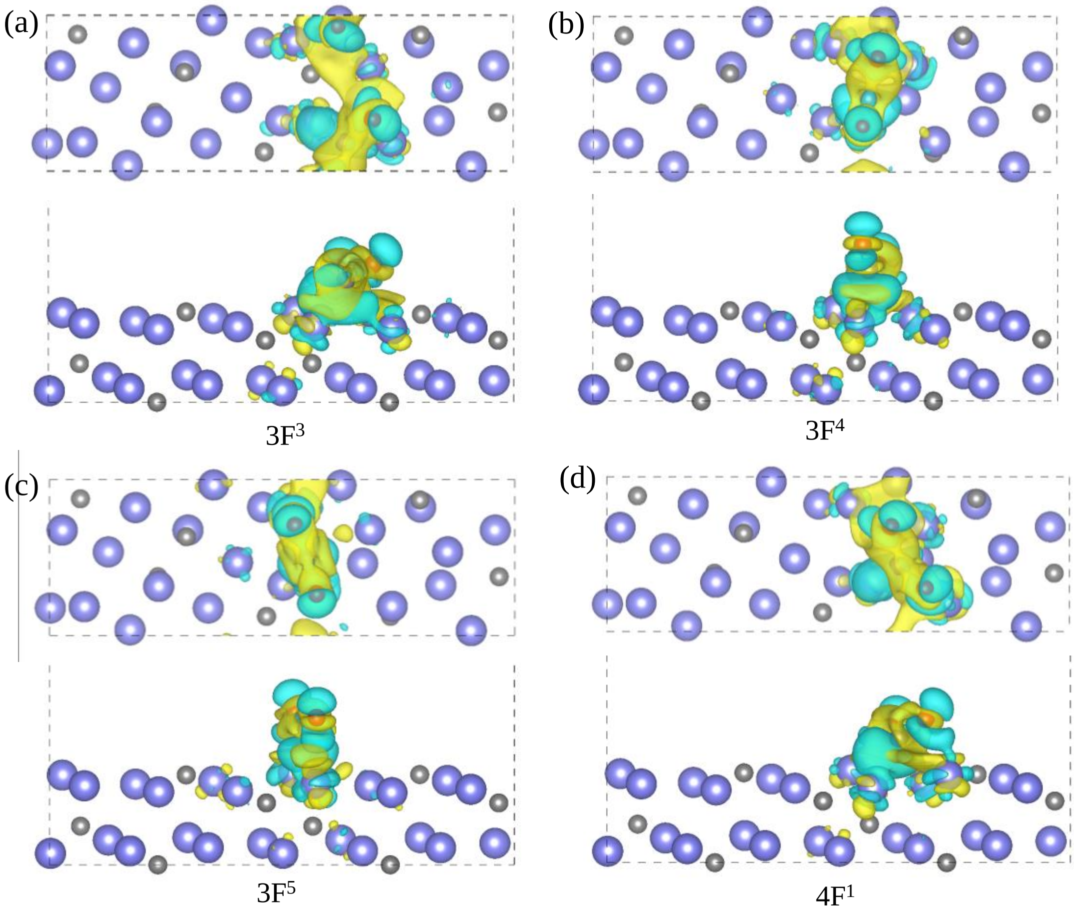

Fig. S7. Top and side views of charge densities for stable CO_2 adsorption structure on χ-Fe_5C_2 (510). (Fe atoms in purple; O atoms in red; C atoms in gray.) Yellow and cyan isosurfaces represent the charge accumulation (i.e. a gain of electron density) and depletion (i.e. a loss of electron density) in the system, respectively.

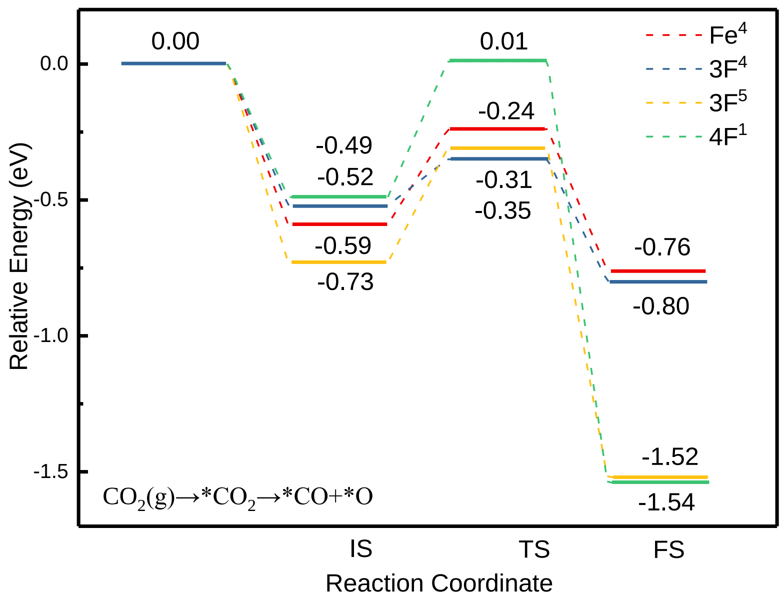

Fig. S8. Potential energy profiles of CO_2 direct dissociation for different configurations on χ-Fe_5C_2 (510) surface.

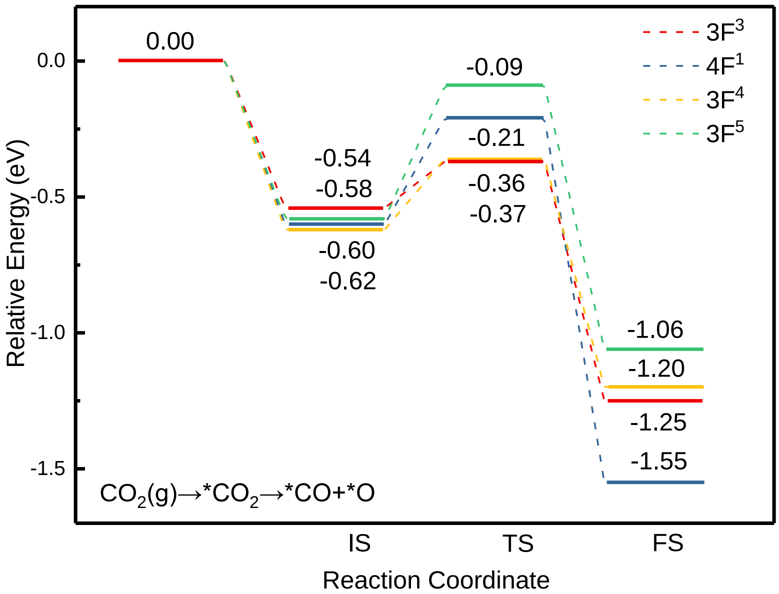

Fig. S9. Potential energy profiles of CO_2 direct dissociation for different configurations on θ-Fe_3C (031) surface.

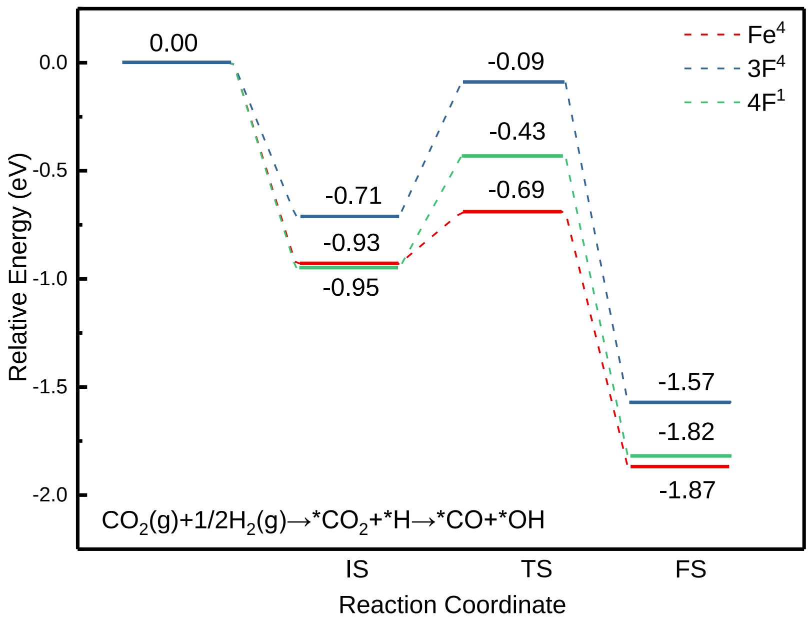

Fig. S10. Potential energy profiles of CO_2 dissociation with H assistance (*CO and *OH pathway) for different configurations on χ-Fe_5C_2 (510) surface.

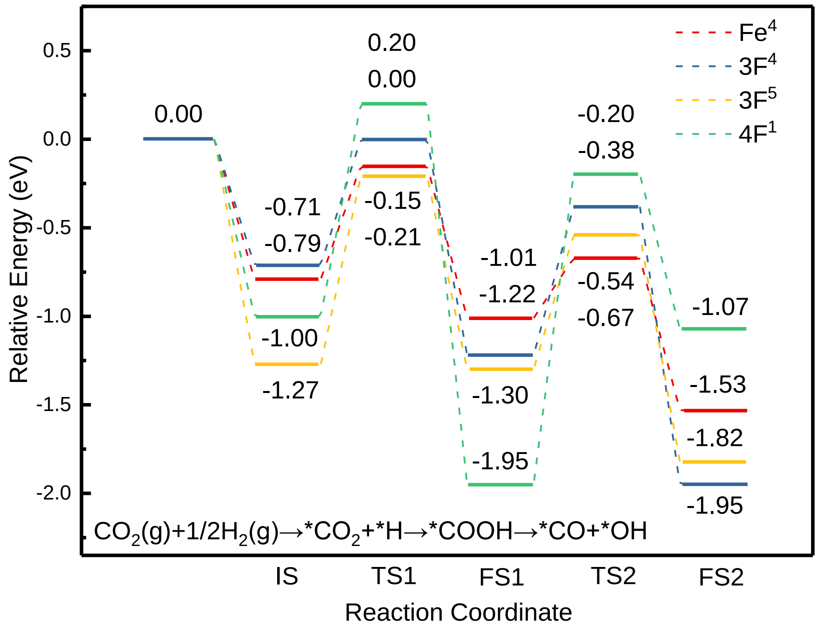

Fig. S11. Potential energy profiles of CO_2 dissociation with H assistance (*COOH pathway) for different configurations on χ-Fe_5C_2 (510) surface.

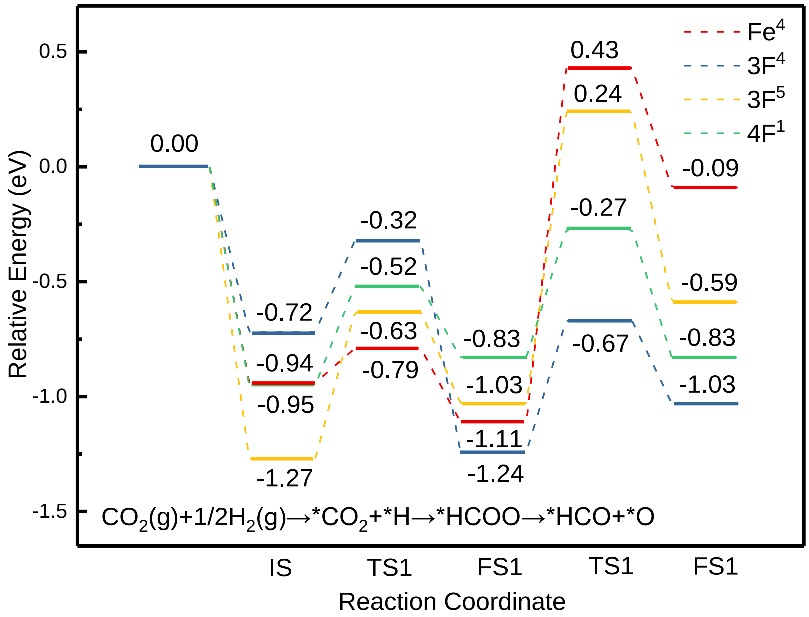

Fig. S12. Potential energy profiles of CO_2 dissociation with H assistance (*HCOO pathway) for different configurations on χ-Fe_5C_2 (510) surface.

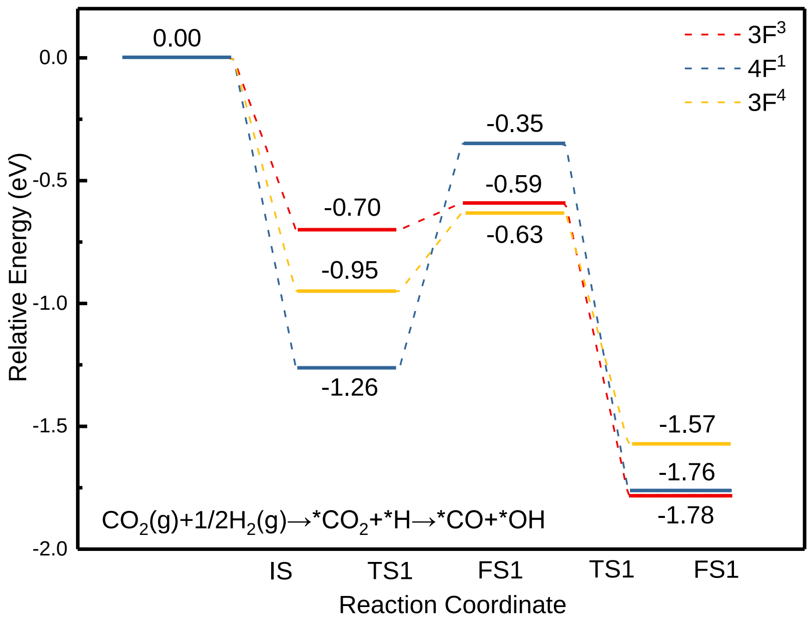

Fig. S13. Potential energy profiles of CO_2 dissociation with H assistance (*CO and *OH pathway) for different configurations on θ-Fe_3C (031) surface.

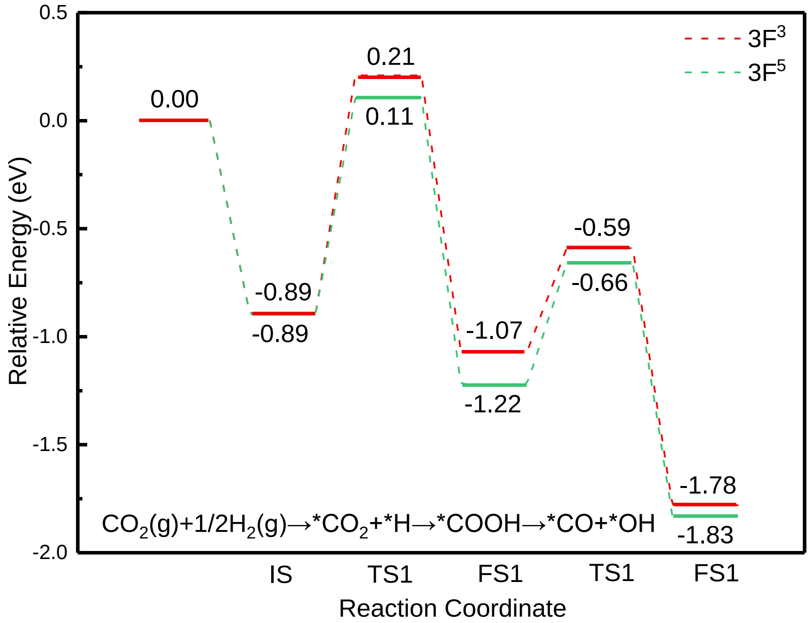

Fig. S14. Potential energy profiles of CO_2 dissociation with H assistance (*COOH pathway) for different configurations on θ-Fe_3C (031) surface.

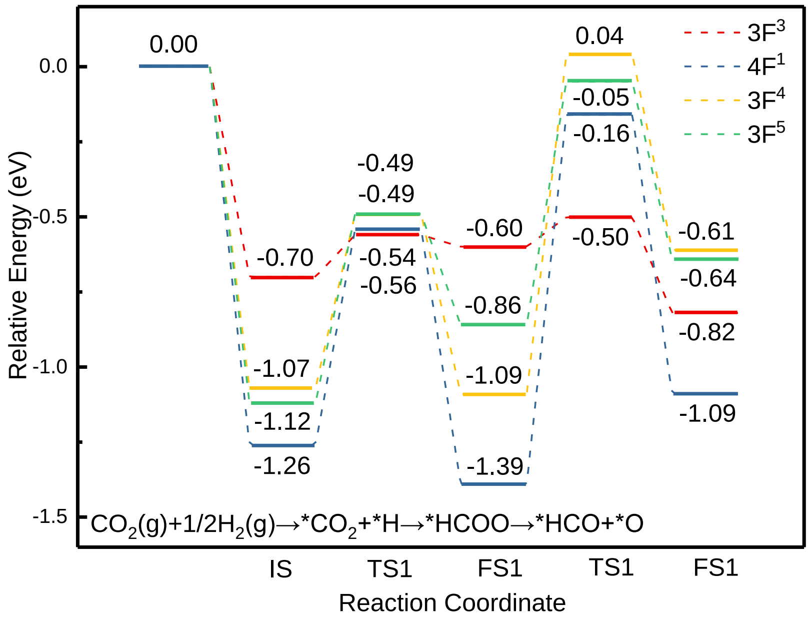

Fig. S15. Potential energy profiles of CO_2 dissociation with H assistance (*HCOO pathway) for different configurations on θ-Fe_3C (031) surface.

Table S1. The lattice parameters of χ-Fe_5C_2 and θ-Fe_3C catalysts in this work and in literatures.

Catalysts	Method	a(Å)	b(Å)	c(Å)	α(°)	β(°)	γ(°)	ref
	Expt.	11.59	4.58	5.06	90.00	97.75	90.00	[16]
	PBE	11.55	4.50	4.98	90.00	97.62	90.00	[17]
χ-Fe_5C_2	PBE	11.58	4.51	4.99	90.00	96.64	90.00	[18]
	PBE	11.56	4.51	4.99	90.00	97.67	90.00	This work
	Expt.	5.09	6.74	4.52	90.00	90.00	90.00	[19]
	PBE	5.00	6.40	4.36	90.00	90.00	90.00	[14]
θ-Fe_3C	PBE	5.03	6.73	4.48	90.00	90.00	90.00	[20]
	PBE	5.03	6.73	4.48	90.00	90.00	90.00	This work

Table S2. Calculated surface energies of different facets of χ-Fe_5C_2 and θ-Fe_3C catalysts.

Phase	Surface	Surface energy (J/m^2)
χ-Fe_5C_2	001	2.72
	010	3.44
	100	3.37
	011	3.01
	101	3.28
	110	3.17
	111	2.80
	510	1.78
θ-Fe_3C	001	2.51
	010	2.56
	100	2.86
	011	2.68
	101	2.51
	110	2.50
	111	2.36
	031	2.27

Table S3. The surface energies of different termination for χ-Fe_5C_2 (510) and θ-Fe_3C (031) surfaces

Surface	Surface termination	Surface energy(J/m^2)
	Mixed termination	1.78
χ-Fe_5C_2 (510)	C-termination	2.43
	Fe-termination	2.43
	Mixed termination	2.27
θ-Fe_3C (031)	C-termination	2.81
	Fe-termination	2.81

Table S4. Influence of slab thickness on CO adsorption energy.

Surface	Thickness (Å)	E_{ads}(eV)	ΔE_{ads}(eV)
χ-Fe_5C_2 (510)	3.93	-2.07	0.01
	5.89	-2.06	
θ-Fe_3C (031)	4.01	-2.05	0.02
	6.02	-2.07	

Table S5. Influence of vacuum heights on CO adsorption energy.

Surface	Thickness (Å)	E_{ads}(eV)	ΔE_{ads}(eV)
χ-Fe_5C_2 (510)	10.5	-2.06	0.00
	12.0	-2.06	
θ-Fe_3C (031)	10.5	-2.05	0.01
	12.0	-2.06	

Table S6. Influence of supercell sizes on CO and CO_2 adsorption energies.

	Supercell size	E_{ads} (eV)	ΔE_{ads}(eV)
χ-Fe_5C_2 (510)			
CO	p(1 × 1)	-2.08	0.00
	p(2 × 1)	-2.08	
CO_2	p(1 × 1)	-0.73	0.00
	p(2 × 1)	-0.73	
θ-Fe_3C (031)			
CO	p(1 × 1)	-2.05	0.05
	p(2 × 1)	-2.10	
CO_2	p(1 × 1)	-0.62	0.03
	p(2 × 1)	-0.65	

Table S7. Influence of Monkhorst−Pack meshes on CO adsorption energy.

Surface	M-P meshes	E_{ads}(eV)	ΔE_{ads}(eV)
χ-Fe_5C_2 (510)	3 × 1 × 1	-2.06	0.00
	5 × 3 × 1	-2.06	
θ-Fe_3C (031)	3 × 1 × 1	-2.05	0.03
	5 × 3 × 1	-2.08	

Tables S8. Adsorption energy and geometric parameters for CO_2 adsorbed on χ-Fe_5C_2 (510) facet.

Sites	E_{ads} (eV)	Angle (°)	d_{C-O} (Å)		d_{C-Fe} (Å)			d_{O-Fe} (Å)			d_{C-C} (Å)
Fe^1	-0.22	140.6	1.24	1.25	1.99	2.33	--	2.11	2.18	--	--
Fe^2	-0.21	137.0	1.24	1.26	2.05	2.24	--	2.04	2.28	--	--
Fe^3	-0.72	125.5	1.30	1.30	1.94	2.09	--	1.96	2.03	--	--
Fe^4	-0.59	126.5	1.23	1.34	2.03	2.23	--	2.00	2.11	--	--
Fe^5	-0.25	179.4	1.17	1.18	--	--	--	2.27	--	--	--
Fe^6	-0.71	137.6	1.25	1.26	1.96	2.24	--	2.05	2.16	--	--
Fe^7	-0.39	132.6	1.22	1.30	2.01	--	--	1.92	--	--	--
Fe^8	-0.29	130.2	1.22	1.31	2.03	--	--	1.89	--	--	--
Fe^9	-0.16	179.9	1.18	1.18	--	--	--	--	--	--	--
Fe^{10}	-0.16	179.5	1.18	1.18	--	--	--	--	--	--	--
$3F^1$	0.09	140.1	1.23	1.25	2.04	2.28	--	2.08	2.28	--	--
$3F^2$	-0.50	123.1	1.31	1.31	1.92	2.27	2.28	2.00	2.18	2.24	--
$3F^3$	-0.55	123.4	1.30	1.32	1.93	2.19	--	2.01	2.04	--	--
$3F^4$	-0.52	131.1	1.23	1.32	1.92	--	--	2.05	2.	--	--
$3F^5$	-0.73	138.8	1.25	1.25	2.00	2.14	--	2.04	2.09	--	--

$3F^{6}$	-0.32	139.7	1.24	1.26	1.94	--	--	2.04	2.29	--	--
$3F^{7}$	-0.22	125.2	1.30	1.30	1.92	2.29	--	2.16	2.25	--	--
$3F^{8}$	-0.14	179.9	1.18	1.18	--	--	--	--	--	--	--
$3F^{9}$	-0.22	137.0	1.24	1.26	2.04	2.24	--	2.04	2.28	--	--
$3F^{10}$	-0.17	136.8	1.24	1.26	2.04	2.23	--	2.04	2.27	--	--
$4F^{1}$	-0.49	128.3	1.22	1.34	2.04	2.17	--	2.03	2.06	--	--
$4F^{2}$	-0.32	126.4	1.21	1.36	2.01	--	--	2.01	2.08	--	--
$4F^{3}$	-0.17	140.7	1.24	1.24	1.99	2.30	--	2.11	2.18	--	--
C_S^{1}	0.34	126.1	1.21	1.39	--	--	--	2.08	2.14	--	1.52
C_S^{2}	-0.06	123.4	1.21	1.39	--	--	--	2.00	2.15	--	1.51

262

Tables S9. Adsorption energy and geometric parameters for CO_2 adsorbed on θ-Fe_3C (031) facet.

Sites	E_{ads} (eV)	Angle (°)	d_{C-O} (Å)		d_{C-Fe} (Å)			d_{O-Fe} (Å)			d_{C-C} (Å)
Fe^{1}	-0.42	138.1	1.24	1.26	1.96	2.28	--	2.04	2.23	--	--
Fe^{2}	-0.36	138.7	1.24	1.26	1.98	2.31	--	2.03	2.23	--	--
Fe^{3}	-0.49	122.6	1.30	1.34	1.94	2.07	--	2.04	2.09	2.14	--
Fe^{4}	-0.56	125.1	1.30	1.30	1.95	2.10	--	1.96	2.02	--	--
Fe^{5}	-0.58	137.2	1.25	1.26	1.98	2.22	--	2.05	2.17	--	--
Fe^{6}	-0.54	138.6	1.24	1.26	1.97	2.20	--	2.05	2.18	--	--
Fe^{7}	-0.42	138.0	1.24	1.26	1.97	2.26	--	2.04	2.22	--	--
Fe^{8}	-0.36	138.8	1.24	1.26	1.97	2.33	--	2.03	2.24	--	--
$3F^{1}$	0.05	138.8	1.24	1.25	2.02	2.29	--	2.09	--	--	--
$3F^{2}$	-0.32	124.0	1.27	1.35	1.90	2.28	2.30	2.07	2.10	2.11	--
$3F^{3}$	-0.54	122.5	1.29	1.34	1.91	2.16	--	2.02	2.05	2.16	--
$3F^{4}$	-0.62	130.8	1.23	1.33	1.93	--	--	2.06	2.10	--	--
$3F^{5}$	0.58	136.9	1.25	1.26	1.99	2.21	--	2.05	2.17	--	--
$3F^{6}$	-0.42	138.0	1.24	1.26	1.96	2.27	--	2.04	2.23	--	--
$4F^{1}$	-0.60	122.4	1.30	1.34	1.91	2.17	--	2.02	2.22	2.28	--
$4F^{2}$	-0.34	136.9	1.23	1.27	1.98	--	--	1.99	--	--	--

C_S[1]	0.36	127.4	1.22	1.34	--	--	--	1.92	--	--	1.54

Table S10. The adsorption properties of reaction intermediates on χ-Fe_5C_2 (510) and θ-Fe_3C (031) surfaces.

COOH		
Facet	χ-Fe_5C_2 (510)	θ-Fe_3C (031)
E_{ads} (eV)	-3.16	-2.86
Bader charge (δ)	0.62	0.50
C-Fe bond length (Å)	1.91	1.90
O-Fe bond length (Å)	1.99	2.03
C-O bond length (Å)	1.33;1.34	1.29;1.35
O-H bond length (Å)	0.99	0.98
O-C-O angle (°)	111.9	113.9
Configuration	mono-dentate	mono-dentate
HCOO		
Facet	χ-Fe_5C_2 (510)	θ-Fe_3C (031)
E_{ads} (eV)	-6.40	-7.18
Bader charge (δ)	0.89	0.62
C-Fe bond length (Å)	2.15;2.29;2.33	--
O-Fe bond length (Å)	1.92;1.96	1.95;2.00
C-O bond length (Å)	1.31;1.32	1.27;1.28
C-H bond length (Å)	1.19	1.11

O-C-O angle (°)	122.5	126.5
Configuration	bi-dentate	bi-dentate
HCO		
Facet	χ-Fe_5C_2 (510)	θ-Fe_3C (031)
E_{ads} (eV)	-3.06	-3.11
Bader charge (δ)	0.72	0.73
C-Fe bond length (Å)	1.89;2.15	1.89;2.11
O-Fe bond length (Å)	1.96;2.18	1.98;2.08
C-O bond length (Å)	1.34	1.35
C-H bond length (Å)	1.11	1.11
CO		
Facet	χ-Fe_5C_2 (510)	θ-Fe_3C (031)
E_{ads} (eV)	-2.09	-2.08
Bader charge (δ)	0.42	0.32
C-Fe bond length (Å)	1.78	1.94;2.04;2.05
C-O bond length (Å)	1.18	1.20
OH		
Facet	χ-Fe_5C_2 (510)	θ-Fe_3C (031)
E_{ads} (eV)	-3.72	-4.02
Bader charge (δ)	0.57	0.58

O-Fe bond length (Å)	1.97;2.00;2.04	1.99;2.00;2.05
O-H bond length (Å)	0.98	0.97

Tables S11. $*CO_2$ dissociation on χ-Fe_5C_2 (510) facet.

	Site	Pathway	E*a*	E*r*
χ-Fe_5C_2 (510)	Fe^{4}	*CO+*O	0.35	-0.17
		*COOH	0.64	-0.74
		*HCOO	1.37	0.85
		*CO+*OH	0.24	-0.94
	$3F^{4}$	*CO+*O	0.17	-0.28
		*COOH	0.71	-1.24
		*HCOO	0.40	-0.31
		*CO+*OH	0.62	-0.86
	$3F^{5}$	*CO+*O	0.42	-0.79
		*COOH	1.06	-0.55
		*HCOO	1.51	-0.68
		*CO+*OH	--	--
	$4F^{1}$	*CO+*O	0.50	-1.05
		*COOH	1.20	-0.07
		*HCOO	0.68	0.12
		*CO+*OH	0.52	-0.87

Tables S12. $^*CO_2$ dissociation on θ-Fe_3C (031) facet.

	Site	Pathway	E*a*	E*r*
θ-Fe_3C (031)	$3F^3$	*CO+*O	0.17	-0.71
		*COOH	1.10	-0.89
		*HCOO	0.20	-0.12
		*CO+*OH	0.11	-1.08
	$3F^4$	*CO+*O	0.26	-0.58
		*COOH	--	--
		*HCOO	1.11	0.46
		*CO+*OH	0.32	-0.62
	$3F^5$	*CO+*O	0.49	-0.48
		*COOH	1.00	-0.94
		*HCOO	1.07	0.48
		*CO+*OH	--	--
	$4F^1$	*CO+*O	0.39	-0.95
		*COOH	--	--
		*HCOO	1.10	0.17
		*CO+*OH	0.91	-0.50

Table S13. The vibrational frequencies for CO_2 direct dissociation on χ-Fe_5C_2 (510) surface

Initial state (IS)				
Site	Fe^4	$3F^4$	$3F^5$	$4F^1$
1f=	1605.43cm^{-1}	1614.99cm^{-1}	1710.49cm^{-1}	1654.57cm^{-1}
2f=	947.64cm^{-1}	1071.60cm^{-1}	1158.43cm^{-1}	936.28cm^{-1}
3f=	678.32cm^{-1}	691.90cm^{-1}	677.34cm^{-1}	673.04cm^{-1}
4f=	389.65cm^{-1}	392.23cm^{-1}	428.98cm^{-1}	414.26cm^{-1}
5f=	297.41cm^{-1}	339.18cm^{-1}	302.60cm^{-1}	292.44cm^{-1}
6f=	158.29cm^{-1}	165.37cm^{-1}	237.35cm^{-1}	178.29cm^{-1}
7f=	148.17cm^{-1}	145.78cm^{-1}	110.44cm^{-1}	151.91cm^{-1}
8f=	93.51cm^{-1}	87.00cm^{-1}	98.67cm^{-1}	133.50cm^{-1}
9f=	53.75cm^{-1}	55.46cm^{-1}	56.20cm^{-1}	92.38cm^{-1}
Transition state (TS)				
1f=	1848.59cm^{-1}	1844.70cm^{-1}	1757.99cm^{-1}	1872.02cm^{-1}
2f=	606.6cm^{-1}	641.28cm^{-1}	682cm^{-1}	601.02cm^{-1}
3f=	428.11cm^{-1}	445.07cm^{-1}	512.60cm^{-1}	437.47cm^{-1}
4f=	372.76cm^{-1}	416.86cm^{-1}	416.96cm^{-1}	387.75cm^{-1}
5f=	284.70cm^{-1}	299.86cm^{-1}	316.60cm^{-1}	270.17cm^{-1}
6f=	219.01cm^{-1}	258.14cm^{-1}	250.41cm^{-1}	207.66cm^{-1}

7f=	$147.68 cm^{-1}$	$99.25 cm^{-1}$	$153.98 cm^{-1}$	$131.30 cm^{-1}$
8f=	$70.03 cm^{-1}$	$37.37 cm^{-1}$	$40.89 cm^{-1}$	$67.46 cm^{-1}$
9f/i=	$387.95 cm^{-1}$	$381.95 cm^{-1}$	$139.95 cm^{-1}$	$418.48 cm^{-1}$
Final state (FS)				
1f=	$1626.12 cm^{-1}$	$1996.99 cm^{-1}$	$1894.12 cm^{-1}$	$1623.15 cm^{-1}$
2f=	$460.86 cm^{-1}$	$579.1 cm^{-1}$	$442.48 cm^{-1}$	$463.12 cm^{-1}$
3f=	$440.25 cm^{-1}$	$426.75 cm^{-1}$	$437.36 cm^{-1}$	$443.75 cm^{-1}$
4f=	$284.89 cm^{-1}$	$416.84 cm^{-1}$	$386.59 cm^{-1}$	$286.01 cm^{-1}$
5f=	$270.54 cm^{-1}$	$390.45 cm^{-1}$	$361.70 cm^{-1}$	$274.30 cm^{-1}$
6f=	$238.71 cm^{-1}$	$379.37 cm^{-1}$	$284.95 cm^{-1}$	$249.08 cm^{-1}$
7f=	$209.88 cm^{-1}$	$207.83 cm^{-1}$	$268.20 cm^{-1}$	$220.36 cm^{-1}$
8f=	$153.83 cm^{-1}$	$66.41 cm^{-1}$	$92.07 cm^{-1}$	$149.29 cm^{-1}$
9f=	$129.41 cm^{-1}$	$58.30 cm^{-1}$	$57.17 cm^{-1}$	$113.82 cm^{-1}$

Table S14. The vibrational frequencies for CO_2 direct dissociation on θ-Fe_3C (031) surface

IS				
Site	$3F^3$	$3F^4$	$3F^5$	$4F^1$
1f=	1298.84cm^{-1}	1620.03cm^{-1}	1679.35cm^{-1}	1295.10cm^{-1}
2f=	1056.96cm^{-1}	1060.75cm^{-1}	1156.98cm^{-1}	1038.93cm^{-1}
3f=	693.71cm^{-1}	686.43cm^{-1}	681.93cm^{-1}	684.75cm^{-1}
4f=	441.26cm^{-1}	388.91cm^{-1}	425.59cm^{-1}	404.79cm^{-1}
5f=	344.86cm^{-1}	344.11cm^{-1}	309.43cm^{-1}	341.10cm^{-1}
6f=	267.58cm^{-1}	190.32cm^{-1}	209.2cm^{-1}	242.16cm^{-1}
7f=	193.11cm^{-1}	152.34cm^{-1}	119.85cm^{-1}	200.39cm^{-1}
8f=	163.05cm^{-1}	93.37cm^{-1}	97.15cm^{-1}	152.88cm^{-1}
9f=	149.02cm^{-1}	80.57cm^{-1}	67.10cm^{-1}	123.59cm^{-1}
TS				
1f=	1828.76cm^{-1}	1816.32cm^{-1}	1809.80cm^{-1}	1802.41cm^{-1}
2f=	633.33cm^{-1}	635.41cm^{-1}	627.65cm^{-1}	618.84cm^{-1}
3f=	433.05cm^{-1}	433.03cm^{-1}	445.01cm^{-1}	395.74cm^{-1}
4f=	411.79cm^{-1}	407.95cm^{-1}	425.24cm^{-1}	364.47cm^{-1}
5f=	303.53cm^{-1}	304.62cm^{-1}	297.27cm^{-1}	309.69cm^{-1}
6f=	261.54cm^{-1}	260.32cm^{-1}	261.99cm^{-1}	264.92cm^{-1}

7f=	102.39cm^{-1}	109.98cm^{-1}	100.21cm^{-1}	127.90cm^{-1}
8f=	46.25cm^{-1}	72.63cm^{-1}	52.64cm^{-1}	53.08cm^{-1}
9f/i=	401.62cm^{-1}	403.49cm^{-1}	422.67cm^{-1}	430.21cm^{-1}
		FS		
1f=	1910.73cm^{-1}	1952.32cm^{-1}	1884.99cm^{-1}	1912.14cm^{-1}
2f=	550.75cm^{-1}	460.83cm^{-1}	504.36cm^{-1}	531.80cm^{-1}
3f=	486.66cm^{-1}	451.98cm^{-1}	431.92cm^{-1}	449.89cm^{-1}
4f=	418.56cm^{-1}	431.82cm^{-1}	385.94cm^{-1}	403.04cm^{-1}
5f=	386.99cm^{-1}	398.58cm^{-1}	372.42cm^{-1}	364.68cm^{-1}
6f=	361.37cm^{-1}	333.29cm^{-1}	314.35cm^{-1}	329.30cm^{-1}
7f=	317.85cm^{-1}	266.17cm^{-1}	246.36cm^{-1}	305.25cm^{-1}
8f=	157.49cm^{-1}	92.82cm^{-1}	73.40cm^{-1}	97.70cm^{-1}
9f=	48.01cm^{-1}	64.84cm^{-1}	48.06cm^{-1}	49.35cm^{-1}

276

Table S15. The vibrational frequencies for CO_2 dissociation with H assistance (*CO and *OH pathway) on χ-Fe_5C_2 (510) surface

		IS		
Site	Fe^4	$3F^4$	$3F^5$	$4F^1$
1f=	1581.15cm^{-1}	2751.75cm^{-1}	--	1672.57cm^{-1}
2f=	1389.24cm^{-1}	1617.55cm^{-1}	--	1221.45cm^{-1}
3f=	995.21cm^{-1}	1087.78cm^{-1}	--	1029.02cm^{-1}
4f=	958.29cm^{-1}	694.19cm^{-1}	--	939.26cm^{-1}
5f=	672.57cm^{-1}	626.05cm^{-1}	--	822.26cm^{-1}
6f=	442.90cm^{-1}	549.31cm^{-1}	--	669.61cm^{-1}
7f=	333.97cm^{-1}	388.15cm^{-1}	--	407.40cm^{-1}
8f=	277.29cm^{-1}	335.58cm^{-1}	--	291.14cm^{-1}
9f=	136.74cm^{-1}	159.23cm^{-1}	--	184.01cm^{-1}
10f=	122.35cm^{-1}	140.23cm^{-1}	--	150.68cm^{-1}
11f=	108.37cm^{-1}	83.46cm^{-1}	--	118.93cm^{-1}
12f=	68.59cm^{-1}	54.36cm^{-1}	--	89.75cm^{-1}
		TS		
1f=	1808.96cm^{-1}	1985.02cm^{-1}	--	1976.79cm^{-1}
2f=	1392.89cm^{-1}	1285.37cm^{-1}	--	967.53cm^{-1}
3f=	947.40cm^{-1}	823.79cm^{-1}	--	630.14cm^{-1}

4f=	608.75cm^{-1}	499.23cm^{-1}	--	567.07cm^{-1}
5f=	427.54cm^{-1}	430.17cm^{-1}	--	470.02cm^{-1}
6f=	409.49cm^{-1}	425.12cm^{-1}	--	445.46cm^{-1}
7f=	375.86cm^{-1}	405.32cm^{-1}	--	429.49cm^{-1}
8f=	281.58cm^{-1}	350.55cm^{-1}	--	372.98cm^{-1}
9f=	209.35cm^{-1}	248.93cm^{-1}	--	274.06cm^{-1}
10f=	151.49cm^{-1}	114.88cm^{-1}	--	101.25cm^{-1}
11f=	77.08cm^{-1}	66.45cm^{-1}	--	60.78cm^{-1}
12f/i=	392.45cm^{-1}	1591.85cm^{-1}	--	650.85cm^{-1}
		FS		
1f=	3685.79cm^{-1}	3682.58cm^{-1}	--	3684.89cm^{-1}
2f=	1934.44cm^{-1}	1925.28cm^{-1}	--	1901.78cm^{-1}
3f=	637.82cm^{-1}	744.95cm^{-1}	--	739.19cm^{-1}
4f=	578.02cm^{-1}	585.56cm^{-1}	--	578.06cm^{-1}
5f=	465.64cm^{-1}	463.06cm^{-1}	--	458.03cm^{-1}
6f=	450.96cm^{-1}	449.41cm^{-1}	--	457.40cm^{-1}
7f=	395.60cm^{-1}	427.78cm^{-1}	--	412.07cm^{-1}
8f=	362.50cm^{-1}	416.76cm^{-1}	--	377.57cm^{-1}
9f=	261.03cm^{-1}	319.79cm^{-1}	--	292.42cm^{-1}
10f=	169.71cm^{-1}	260.83cm^{-1}	--	167.93cm^{-1}

11f=	100.81cm^{-1}	117.55cm^{-1}	--	91.90cm^{-1}
12f=	42.40cm^{-1}	50.22cm^{-1}	--	38.15cm^{-1}

Table S16. The vibrational frequencies for CO_2 dissociation with H assistance (*COOH pathway) on χ-Fe_5C_2 (510) surface

		IS		
Site	Fe^4	$3F^4$	$3F^5$	$4F^1$
1f=	1669.91cm^{-1}	2751.75cm^{-1}	1724.36cm^{-1}	1672.57cm^{-1}
2f=	1390.81cm^{-1}	1617.55cm^{-1}	1178.70cm^{-1}	1221.45cm^{-1}
3f=	936.47cm^{-1}	1087.78cm^{-1}	1168.07cm^{-1}	1029.02cm^{-1}
4f=	866.68cm^{-1}	694.19cm^{-1}	1055.61cm^{-1}	939.26cm^{-1}
5f=	683.92cm^{-1}	626.05cm^{-1}	800.58cm^{-1}	822.26cm^{-1}
6f=	629.46cm^{-1}	549.31cm^{-1}	675.01cm^{-1}	669.61cm^{-1}
7f=	461.44cm^{-1}	388.15cm^{-1}	440.88cm^{-1}	407.40cm^{-1}
8f=	313.37cm^{-1}	335.58cm^{-1}	296.20cm^{-1}	291.14cm^{-1}
9f=	194.83cm^{-1}	159.23cm^{-1}	235.51cm^{-1}	184.01cm^{-1}
10f=	193.77cm^{-1}	140.23cm^{-1}	114.00cm^{-1}	150.68cm^{-1}
11f=	158.64cm^{-1}	83.46cm^{-1}	97.31cm^{-1}	118.93cm^{-1}
12f=	68.47cm^{-1}	54.36cm^{-1}	79.89cm^{-1}	89.75cm^{-1}
		TS1		
1f=	1445.47cm^{-1}	1481.95cm^{-1}	1590.53cm^{-1}	1461.04cm^{-1}
2f=	1106.77cm^{-1}	1174.87cm^{-1}	1176.26cm^{-1}	1318.87cm^{-1}
3f=	982.05cm^{-1}	1004.06cm^{-1}	1078.21cm^{-1}	1106.11cm^{-1}

4f=	699.84cm^{-1}	708.27cm^{-1}	689.02cm^{-1}	676.04cm^{-1}
5f=	603.92cm^{-1}	532.91cm^{-1}	614.74cm^{-1}	533.32cm^{-1}
6f=	388.26cm^{-1}	411.72cm^{-1}	360.67cm^{-1}	389.23cm^{-1}
7f=	306.16cm^{-1}	339.34cm^{-1}	302.08cm^{-1}	298.40cm^{-1}
8f=	258.97cm^{-1}	277.47cm^{-1}	287.13cm^{-1}	201.62cm^{-1}
9f=	179.71cm^{-1}	153.41cm^{-1}	119.08cm^{-1}	164.19cm^{-1}
10f=	112.78cm^{-1}	89.16cm^{-1}	113.16cm^{-1}	118.92cm^{-1}
11f=	108.13cm^{-1}	66.59cm^{-1}	70.41cm^{-1}	37.87cm^{-1}
12f/i=	1363.26cm^{-1}	1345.82cm^{-1}	1326.56cm^{-1}	1453.00cm^{-1}
		FS1		
1f=	3598.51cm^{-1}	3570.70cm^{-1}	3566.77cm^{-1}	3648.43cm^{-1}
2f=	1315.03cm^{-1}	1308.02cm^{-1}	1310.78cm^{-1}	1302.17cm^{-1}
3f=	1202.76cm^{-1}	1204.39cm^{-1}	1202.64cm^{-1}	1198.11cm^{-1}
4f=	1081.59cm^{-1}	1078.98cm^{-1}	1084.23cm^{-1}	1076.14cm^{-1}
5f=	680.01cm^{-1}	692.31cm^{-1}	695.73cm^{-1}	672.37cm^{-1}
6f=	559.60cm^{-1}	686.34cm^{-1}	691.21cm^{-1}	523.69cm^{-1}
7f=	462.80cm^{-1}	469.08cm^{-1}	465.82cm^{-1}	422.18cm^{-1}
8f=	317.68cm^{-1}	350.43cm^{-1}	351.29cm^{-1}	311.60cm^{-1}
9f=	246.75cm^{-1}	261.01cm^{-1}	260.15cm^{-1}	239.58cm^{-1}
10f=	174.28cm^{-1}	161.65cm^{-1}	161.84cm^{-1}	184.78cm^{-1}

11f=	154.45cm^{-1}	114.03cm^{-1}	104.06cm^{-1}	134.44cm^{-1}
12f=	59.07cm^{-1}	76.46cm^{-1}	79.60cm^{-1}	83.97cm^{-1}
		TS2		
1f=	3609.14cm^{-1}	3488.03cm^{-1}	3518.65cm^{-1}	3534.52cm^{-1}
2f=	1384.27cm^{-1}	1557.85cm^{-1}	1552.49cm^{-1}	1671.53cm^{-1}
3f=	1190.60cm^{-1}	1070.24cm^{-1}	1197.69cm^{-1}	903.82cm^{-1}
4f=	1095.83cm^{-1}	845.08cm^{-1}	1014.41cm^{-1}	709.67cm^{-1}
5f=	687.40cm^{-1}	573.36cm^{-1}	617.74cm^{-1}	611.45cm^{-1}
6f=	580.37cm^{-1}	520.58cm^{-1}	530.70cm^{-1}	434.22cm^{-1}
7f=	464.81cm^{-1}	304.16cm^{-1}	345.59cm^{-1}	366.36cm^{-1}
8f=	337.01cm^{-1}	232.69cm^{-1}	227.92cm^{-1}	266.35cm^{-1}
9f=	250.18cm^{-1}	142.92cm^{-1}	106.29cm^{-1}	192.81cm^{-1}
10f=	160.19cm^{-1}	102.90cm^{-1}	81.49cm^{-1}	93.16cm^{-1}
11f=	94.98cm^{-1}	53.98cm^{-1}	56.02cm^{-1}	67.81cm^{-1}
12f/i=	184.51cm^{-1}	193.68cm^{-1}	129.90cm^{-1}	242.70cm^{-1}
		FS2		
1f=	3526.96cm^{-1}	3740.15cm^{-1}	3724.18cm^{-1}	3746.58cm^{-1}
2f=	1589.90cm^{-1}	1922.14cm^{-1}	1704.18cm^{-1}	1688.28cm^{-1}
3f=	673.66cm^{-1}	591.54cm^{-1}	626.60cm^{-1}	656.37cm^{-1}
4f=	581.94cm^{-1}	516.60cm^{-1}	554.77cm^{-1}	564.90cm^{-1}

5f=	420.75cm^{-1}	449.76cm^{-1}	430.87cm^{-1}	442.67cm^{-1}
6f=	390.47cm^{-1}	437.15cm^{-1}	381.14cm^{-1}	314.53cm^{-1}
7f=	313.98cm^{-1}	429.08cm^{-1}	318.15cm^{-1}	278.55cm^{-1}
8f=	278.51cm^{-1}	409.15cm^{-1}	293.02cm^{-1}	245.74cm^{-1}
9f=	244.51cm^{-1}	293.54cm^{-1}	275.88cm^{-1}	217.09cm^{-1}
10f=	226.36cm^{-1}	262.89cm^{-1}	249.96cm^{-1}	183.97cm^{-1}
11f=	166.77cm^{-1}	65.59cm^{-1}	136.37cm^{-1}	132.84cm^{-1}
12f=	133.53cm^{-1}	45.97cm^{-1}	126.06cm^{-1}	108.39cm^{-1}

Table S17. The vibrational frequencies for CO_2 dissociation with H assistance (*HCOO pathway) on χ-Fe_5C_2 (510) surface

IS				
Site	Fe^4	$3F^4$	$3F^5$	$4F^1$
1f=	1651.15cm^{-1}	1628.50cm^{-1}	1724.36cm^{-1}	1656.00cm^{-1}
2f=	1270.17cm^{-1}	1227.66cm^{-1}	1178.70cm^{-1}	1219.87cm^{-1}
3f=	1084.96cm^{-1}	1066.13cm^{-1}	1168.07cm^{-1}	1025.77cm^{-1}
4f=	994.61cm^{-1}	985.33cm^{-1}	1055.61cm^{-1}	994.69cm^{-1}
5f=	749.96cm^{-1}	688.57cm^{-1}	800.58cm^{-1}	672.21cm^{-1}
6f=	670.46cm^{-1}	646.73cm^{-1}	675.01cm^{-1}	652.93cm^{-1}
7f=	460.11cm^{-1}	381.59cm^{-1}	440.88cm^{-1}	409.91cm^{-1}
8f=	287.89cm^{-1}	329.62cm^{-1}	296.20cm^{-1}	282.08cm^{-1}
9f=	216.92cm^{-1}	187.16cm^{-1}	235.51cm^{-1}	174.56cm^{-1}
10f=	154.39cm^{-1}	141.58cm^{-1}	114.00cm^{-1}	151.83cm^{-1}
11f=	123.02cm^{-1}	94.83cm^{-1}	97.31cm^{-1}	118.09cm^{-1}
12f=	77.03cm^{-1}	34.95cm^{-1}	79.89cm^{-1}	100.71cm^{-1}
TS1				
1f=	1735.5cm^{-1}	1784.70cm^{-1}	1794.99cm^{-1}	2472.45cm^{-1}
2f=	1384.51cm^{-1}	1400.44cm^{-1}	1403.77cm^{-1}	1311.43cm^{-1}
3f=	1092.89cm^{-1}	1100.35cm^{-1}	1100.36cm^{-1}	1173.90cm^{-1}

4f=	836.19cm^{-1}	687.39cm^{-1}	722.86cm^{-1}	1086.78cm^{-1}
5f=	809.66cm^{-1}	589.73cm^{-1}	665.15cm^{-1}	801.16cm^{-1}
6f=	636.54cm^{-1}	522.15cm^{-1}	520.66cm^{-1}	627.47cm^{-1}
7f=	367.84cm^{-1}	335.94cm^{-1}	332.14cm^{-1}	337.29cm^{-1}
8f=	285.08cm^{-1}	296.59cm^{-1}	303.62cm^{-1}	323.98cm^{-1}
9f=	245.14cm^{-1}	190.38cm^{-1}	180.34cm^{-1}	300.09cm^{-1}
10f=	207.45cm^{-1}	153.82cm^{-1}	162.57cm^{-1}	161.68cm^{-1}
11f=	68.67cm^{-1}	128.42cm^{-1}	130.56cm^{-1}	106.71cm^{-1}
12f/i=	152.47cm^{-1}	609.68cm^{-1}	714.85cm^{-1}	142.01cm^{-1}
		FS1		
1f=	2960.80cm^{-1}	3028.33cm^{-1}	2828.91cm^{-1}	2985.31cm^{-1}
2f=	1677.98cm^{-1}	1274.43cm^{-1}	1316.58cm^{-1}	1306.68cm^{-1}
3f=	1321.40cm^{-1}	1175.16cm^{-1}	1243.59cm^{-1}	1265.29cm^{-1}
4f=	1115.73cm^{-1}	1066.81cm^{-1}	1148.53cm^{-1}	1107.69cm^{-1}
5f=	988.69cm^{-1}	820.63cm^{-1}	848.91cm^{-1}	807.14cm^{-1}
6f=	719.59cm^{-1}	613.92cm^{-1}	622.06cm^{-1}	604.83cm^{-1}
7f=	328.52cm^{-1}	475.15cm^{-1}	446.28cm^{-1}	417.46cm^{-1}
8f=	248.83cm^{-1}	386.72cm^{-1}	386.88cm^{-1}	376.20cm^{-1}
9f=	181.57cm^{-1}	301.39cm^{-1}	229.86cm^{-1}	262.16cm^{-1}
10f=	110.36cm^{-1}	228.03cm^{-1}	131.57cm^{-1}	171.76cm^{-1}

11f=	48.14cm^{-1}	126.91cm^{-1}	115.56cm^{-1}	141.85cm^{-1}
12f=	17.58cm^{-1}	90.84cm^{-1}	87.93cm^{-1}	108.38cm^{-1}
		TS2		
1f=	2965.27cm^{-1}	2939.69cm^{-1}	2989.81cm^{-1}	2875.97cm^{-1}
2f=	1242.80cm^{-1}	1214.93cm^{-1}	1318.68cm^{-1}	1424.94cm^{-1}
3f=	1111.92cm^{-1}	1195.09cm^{-1}	1147.58cm^{-1}	1177.43cm^{-1}
4f=	765.34cm^{-1}	672.40cm^{-1}	842.76cm^{-1}	702.90cm^{-1}
5f=	526.28cm^{-1}	525.00cm^{-1}	705.86cm^{-1}	558.07cm^{-1}
6f=	426.30cm^{-1}	489.13cm^{-1}	487.16cm^{-1}	519.53cm^{-1}
7f=	322.74cm^{-1}	456.54cm^{-1}	353.50cm^{-1}	468.23cm^{-1}
8f=	272.15cm^{-1}	367.61cm^{-1}	307.48cm^{-1}	304.73cm^{-1}
9f=	239.02cm^{-1}	297.16cm^{-1}	164.88cm^{-1}	258.48cm^{-1}
10f=	221.16cm^{-1}	199.06cm^{-1}	120.61cm^{-1}	171.80cm^{-1}
11f=	196.69cm^{-1}	144.00cm^{-1}	74.67cm^{-1}	143.83cm^{-1}
12f/i=	176.47cm^{-1}	158.24cm^{-1}	344.63cm^{-1}	172.38cm^{-1}
		FS2		
1f=	3034.81cm^{-1}	3740.15cm^{-1}	2890.53cm^{-1}	2921.68cm^{-1}
2f=	1241.56cm^{-1}	1922.14cm^{-1}	1277.56cm^{-1}	1181.88cm^{-1}
3f=	986.18cm^{-1}	591.54cm^{-1}	1179.62cm^{-1}	1162.12cm^{-1}
4f=	801.58cm^{-1}	516.60cm^{-1}	688.52cm^{-1}	684.90cm^{-1}

5f=	643.88cm^{-1}	449.76cm^{-1}	508.95cm^{-1}	544.31cm^{-1}
6f=	423.01cm^{-1}	437.15cm^{-1}	491.27cm^{-1}	508.74cm^{-1}
7f=	417.37cm^{-1}	429.08cm^{-1}	378.42cm^{-1}	405.96cm^{-1}
8f=	393.68cm^{-1}	409.15cm^{-1}	375.29cm^{-1}	362.35cm^{-1}
9f=	277.26cm^{-1}	293.54cm^{-1}	262.51cm^{-1}	343.36cm^{-1}
10f=	266.87cm^{-1}	262.89cm^{-1}	194.11cm^{-1}	316.99cm^{-1}
11f=	217.44cm^{-1}	65.59cm^{-1}	133.54cm^{-1}	275.17cm^{-1}
12f=	160.00cm^{-1}	45.97cm^{-1}	89.73cm^{-1}	215.64cm^{-1}

Table S18. The vibrational frequencies for CO_2 dissociation with H assistance (*CO and *OH pathway) on θ-Fe_3C (031) surface

IS				
Site	$3F^3$	$3F^4$	$3F^5$	$4F^1$
1f=	1523.09cm^{-1}	1672.13cm^{-1}	--	1312.70cm^{-1}
2f=	1356.58cm^{-1}	1528.09cm^{-1}	--	1258.23cm^{-1}
3f=	1072.61cm^{-1}	1092.36cm^{-1}	--	1066.51cm^{-1}
4f=	950.52cm^{-1}	847.05cm^{-1}	--	972.02cm^{-1}
5f=	694.49cm^{-1}	676.54cm^{-1}	--	789.26cm^{-1}
6f=	575.39cm^{-1}	495.94cm^{-1}	--	688.48cm^{-1}
7f=	468.92cm^{-1}	345.06cm^{-1}	--	437.69cm^{-1}
8f=	316.21cm^{-1}	337.12cm^{-1}	--	344.56cm^{-1}
9f=	274.03cm^{-1}	236.30cm^{-1}	--	253.09cm^{-1}
10f=	204.89cm^{-1}	179.18cm^{-1}	--	205.56cm^{-1}
11f=	188.68cm^{-1}	125.09cm^{-1}	--	160.78cm^{-1}
12f=	131.97cm^{-1}	76.40cm^{-1}	--	133.51cm^{-1}
TS				
1f=	1916.02cm^{-1}	1958.99cm^{-1}	--	1863.86cm^{-1}
2f=	1324.54cm^{-1}	1026.60cm^{-1}	--	1353.61cm^{-1}
3f=	562.82cm^{-1}	740.47cm^{-1}	--	594.96cm^{-1}

4f=	522.90cm^{-1}	541.63cm^{-1}	--	508.25cm^{-1}
5f=	453.85cm^{-1}	460.27cm^{-1}	--	424.68cm^{-1}
6f=	383.94cm^{-1}	433.36cm^{-1}	--	316.10cm^{-1}
7f=	367.23cm^{-1}	400.95cm^{-1}	--	299.61cm^{-1}
8f=	360.85cm^{-1}	351.23cm^{-1}	--	262.87cm^{-1}
9f=	188.00cm^{-1}	249.22cm^{-1}	--	202.26cm^{-1}
10f=	102.89cm^{-1}	105.00cm^{-1}	--	79.51cm^{-1}
11f=	55.01cm^{-1}	68.62cm^{-1}	--	58.68cm^{-1}
12f/i=	1263.16cm^{-1}	1092.97cm^{-1}	--	1355.81cm^{-1}
		FS		
1f=	3464.11cm^{-1}	3674.25cm^{-1}	--	3582.12cm^{-1}
2f=	1708.89cm^{-1}	1935.76cm^{-1}	--	1784.47cm^{-1}
3f=	801.54cm^{-1}	755.55cm^{-1}	--	696.28cm^{-1}
4f=	769.08cm^{-1}	629.77cm^{-1}	--	659.07cm^{-1}
5f=	504.95cm^{-1}	468.95cm^{-1}	--	489.76cm^{-1}
6f=	441.74cm^{-1}	434.68cm^{-1}	--	444.86cm^{-1}
7f=	334.38cm^{-1}	417.92cm^{-1}	--	348.98cm^{-1}
8f=	309.95cm^{-1}	409.88cm^{-1}	--	322.62cm^{-1}
9f=	280.57cm^{-1}	295.02cm^{-1}	--	252.25cm^{-1}
10f=	235.11cm^{-1}	241.18cm^{-1}	--	205.63cm^{-1}

11f=	120.20cm^{-1}	98.72cm^{-1}	--	108.96cm^{-1}
12f=	98.55cm^{-1}	56.79cm^{-1}	--	75.77cm^{-1}

Table S19. The vibrational frequencies for CO_2 dissociation with H assistance (*COOH pathway) on θ-Fe_3C (031) surface

		IS		
Site	$3F^3$	$3F^4$	$3F^5$	$4F^1$
1f=	1330.14cm^{-1}	--	1717.94cm^{-1}	--
2f=	1321.51cm^{-1}	--	1160.33cm^{-1}	--
3f=	1075.61cm^{-1}	--	962.77cm^{-1}	--
4f=	919.11cm^{-1}	--	786.31cm^{-1}	--
5f=	761.73cm^{-1}	--	663.32cm^{-1}	--
6f=	706.32cm^{-1}	--	582.58cm^{-1}	--
7f=	431.41cm^{-1}	--	443.01cm^{-1}	--
8f=	340.55cm^{-1}	--	288.69cm^{-1}	--
9f=	270.41cm^{-1}	--	204.57cm^{-1}	--
10f=	196.89cm^{-1}	--	124.58cm^{-1}	--
11f=	166.38cm^{-1}	--	102.67cm^{-1}	--
12f=	78.93cm^{-1}	--	73.82cm^{-1}	--
		TS1		
1f=	1243.12cm^{-1}	--	1484.42cm^{-1}	--
2f=	1215.22cm^{-1}	--	1183.74cm^{-1}	--
3f=	1084.41cm^{-1}	--	1098.87cm^{-1}	--

4f=	686.54cm^{-1}	--	712.51cm^{-1}	--
5f=	677.02cm^{-1}	--	504.00cm^{-1}	--
6f=	408.96cm^{-1}	--	432.36cm^{-1}	--
7f=	339.99cm^{-1}	--	332.49cm^{-1}	--
8f=	238.15cm^{-1}	--	251.09cm^{-1}	--
9f=	175.01cm^{-1}	--	153.16cm^{-1}	--
10f=	171.23cm^{-1}	--	102.85cm^{-1}	--
11f=	68.98cm^{-1}	--	59.81cm^{-1}	--
12f/i=	1401.78cm^{-1}	--	1315.68cm^{-1}	--
		FS1		
1f=	3529.63cm^{-1}	--	3579.35cm^{-1}	--
2f=	1288.01cm^{-1}	--	1295.40cm^{-1}	--
3f=	1219.35cm^{-1}	--	1203.33cm^{-1}	--
4f=	1038.82cm^{-1}	--	1060.75cm^{-1}	--
5f=	656.52cm^{-1}	--	682.85cm^{-1}	--
6f=	615.44cm^{-1}	--	671.03cm^{-1}	--
7f=	446.13cm^{-1}	--	478.70cm^{-1}	--
8f=	357.02cm^{-1}	--	353.43cm^{-1}	--
9f=	254.55cm^{-1}	--	270.29cm^{-1}	--
10f=	169.41cm^{-1}	--	183.88cm^{-1}	--

11f=	151.17cm^{-1}	--	140.61cm^{-1}	--
12f=	86.60cm^{-1}	--	81.47cm^{-1}	--
		TS2		
1f=	3531.94cm^{-1}	--	3687.68cm^{-1}	--
2f=	1564.85cm^{-1}	--	1178.07cm^{-1}	--
3f=	1130.39cm^{-1}	--	1123.78cm^{-1}	--
4f=	888.19cm^{-1}	--	972.93cm^{-1}	--
5f=	613.72cm^{-1}	--	666.33cm^{-1}	--
6f=	554.53cm^{-1}	--	442.99cm^{-1}	--
7f=	443.27cm^{-1}	--	359.73cm^{-1}	--
8f=	297.88cm^{-1}	--	221.01cm^{-1}	--
9f=	237.78cm^{-1}	--	197.99cm^{-1}	--
10f=	94.40cm^{-1}	--	127.04cm^{-1}	--
11f=	54.34cm^{-1}	--	66.13cm^{-1}	--
12f/i=	100.25cm^{-1}	--	591.83cm^{-1}	--
		FS2		
1f=	3641.25cm^{-1}	--	3682.46cm^{-1}	--
2f=	1719.00cm^{-1}	--	1890.51cm^{-1}	--
3f=	756.56cm^{-1}	--	676.58cm^{-1}	--
4f=	651.22cm^{-1}	--	560.21cm^{-1}	--

5f=	405.39cm^{-1}	--	446.98cm^{-1}	--
6f=	392.94cm^{-1}	--	425.27cm^{-1}	--
7f=	291.09cm^{-1}	--	412.72cm^{-1}	--
8f=	252.04cm^{-1}	--	383.58cm^{-1}	--
9f=	208.63cm^{-1}	--	244.21cm^{-1}	--
10f=	159.12cm^{-1}	--	164.83cm^{-1}	--
11f=	148.45cm^{-1}	--	67.02cm^{-1}	--
12f=	47.45cm^{-1}	--	50.88cm^{-1}	--

291

Table S20. The vibrational frequencies for CO_2 dissociation with H assistance (*HCOO pathway) on θ-Fe_3C (031) surface

		IS		
Site	$3F^3$	$3F^4$	$3F^5$	$4F^1$
1f=	1523.09cm^{-1}	1627.67cm^{-1}	1699.40cm^{-1}	1312.70cm^{-1}
2f=	1356.58cm^{-1}	1166.11cm^{-1}	1170.45cm^{-1}	1258.23cm^{-1}
3f=	1072.61cm^{-1}	1096.68cm^{-1}	1163.5cm^{-1}	1066.51cm^{-1}
4f=	950.52cm^{-1}	1089.95cm^{-1}	1056.56cm^{-1}	972.02cm^{-1}
5f=	694.49cm^{-1}	769.13cm^{-1}	789.41cm^{-1}	789.26cm^{-1}
6f=	575.39cm^{-1}	687.20cm^{-1}	675.40cm^{-1}	688.48cm^{-1}
7f=	468.92cm^{-1}	394.65cm^{-1}	433.82cm^{-1}	437.69cm^{-1}
8f=	316.21cm^{-1}	331.41cm^{-1}	302.40cm^{-1}	344.56cm^{-1}
9f=	274.03cm^{-1}	171.84cm^{-1}	209.89cm^{-1}	253.09cm^{-1}
10f=	204.89cm^{-1}	144.89cm^{-1}	121.90cm^{-1}	205.56cm^{-1}
11f=	188.68cm^{-1}	101.70cm^{-1}	92.11cm^{-1}	160.78cm^{-1}
12f=	131.97cm^{-1}	71.00cm^{-1}	77.00cm^{-1}	133.51cm^{-1}
		TS1		
1f=	1788.19cm^{-1}	1766.54cm^{-1}	1780.38cm^{-1}	1847.98cm^{-1}
2f=	1289.36cm^{-1}	1394.21cm^{-1}	1395.91cm^{-1}	1278.50cm^{-1}
3f=	1015.31cm^{-1}	1098.15cm^{-1}	1100.22cm^{-1}	1130.98cm^{-1}

4f=	794.38cm^{-1}	724.20cm^{-1}	726.36cm^{-1}	1057.76cm^{-1}
5f=	685.26cm^{-1}	662.13cm^{-1}	664.28cm^{-1}	982.74cm^{-1}
6f=	557.03cm^{-1}	512.40cm^{-1}	513.49cm^{-1}	638.37cm^{-1}
7f=	322.40cm^{-1}	332.96cm^{-1}	336.55cm^{-1}	355.34cm^{-1}
8f=	300.27cm^{-1}	280.37cm^{-1}	277.72cm^{-1}	282.26cm^{-1}
9f=	236.33cm^{-1}	181.66cm^{-1}	185.62cm^{-1}	241.50cm^{-1}
10f=	205.04cm^{-1}	157.35cm^{-1}	160.52cm^{-1}	169.49cm^{-1}
11f=	146.64cm^{-1}	125.77cm^{-1}	127.36cm^{-1}	124.39cm^{-1}
12f/i=	467.16cm^{-1}	727.46cm^{-1}	718.27cm^{-1}	304.67cm^{-1}
		FS1		
1f=	1840.86cm^{-1}	3009.53cm^{-1}	2873.33cm^{-1}	3043.66cm^{-1}
2f=	1280.84cm^{-1}	1306.77cm^{-1}	1314.82cm^{-1}	1296.56cm^{-1}
3f=	1234.69cm^{-1}	1238.07cm^{-1}	1248.35cm^{-1}	1179.45cm^{-1}
4f=	984.27cm^{-1}	1115.12cm^{-1}	1147.78cm^{-1}	1090.17cm^{-1}
5f=	954.53cm^{-1}	832.04cm^{-1}	835.65cm^{-1}	806.47cm^{-1}
6f=	610.30cm^{-1}	635.18cm^{-1}	622.52cm^{-1}	627.99cm^{-1}
7f=	342.87cm^{-1}	449.66cm^{-1}	446.65cm^{-1}	465.41cm^{-1}
8f=	321.64cm^{-1}	365.20cm^{-1}	386.27cm^{-1}	367.26cm^{-1}
9f=	305.96cm^{-1}	253.11cm^{-1}	213.62cm^{-1}	305.55cm^{-1}
10f=	231.03cm^{-1}	191.60cm^{-1}	117.76cm^{-1}	276.64cm^{-1}

11f=	162.94cm^{-1}	114.16cm^{-1}	105.07cm^{-1}	217.61cm^{-1}
12f=	145.06cm^{-1}	101.89cm^{-1}	76.16cm^{-1}	124.56cm^{-1}
		TS2		
1f=	2983.00cm^{-1}	3009.97cm^{-1}	3014.75cm^{-1}	2976.54cm^{-1}
2f=	1406.93cm^{-1}	1202.86cm^{-1}	1236.30cm^{-1}	1290.53cm^{-1}
3f=	1169.10cm^{-1}	1164.71cm^{-1}	1193.62cm^{-1}	1170.07cm^{-1}
4f=	915.98cm^{-1}	872.18cm^{-1}	880.73cm^{-1}	745.58cm^{-1}
5f=	508.08cm^{-1}	535.68cm^{-1}	555.61cm^{-1}	497.85cm^{-1}
6f=	464.74cm^{-1}	520.13cm^{-1}	506.52cm^{-1}	449.71cm^{-1}
7f=	420.38cm^{-1}	377.46cm^{-1}	362.04cm^{-1}	382.62cm^{-1}
8f=	299.27cm^{-1}	296.57cm^{-1}	312.45cm^{-1}	312.51cm^{-1}
9f=	296.77cm^{-1}	209.23cm^{-1}	264.07cm^{-1}	279.45cm^{-1}
10f=	213.78cm^{-1}	176.60cm^{-1}	173.23cm^{-1}	200.92cm^{-1}
11f=	142.79cm^{-1}	95.72cm^{-1}	99.21cm^{-1}	171.52cm^{-1}
12f/i=	326.91cm^{-1}	386.35cm^{-1}	411.81cm^{-1}	234.31cm^{-1}
		FS2		
1f=	2861.08cm^{-1}	2954.60cm^{-1}	2863.82cm^{-1}	2931.93cm^{-1}
2f=	1460.47cm^{-1}	1183.69cm^{-1}	1306.30cm^{-1}	1191.72cm^{-1}
3f=	1163.18cm^{-1}	1118.65cm^{-1}	1181.01cm^{-1}	1063.72cm^{-1}
4f=	742.81cm^{-1}	735.35cm^{-1}	735.18cm^{-1}	725.83cm^{-1}

5f=	579.12cm^{-1}	572.43cm^{-1}	507.77cm^{-1}	520.92cm^{-1}
6f=	389.88cm^{-1}	570.00cm^{-1}	490.42cm^{-1}	481.77cm^{-1}
7f=	329.44cm^{-1}	383.85cm^{-1}	373.14cm^{-1}	466.84cm^{-1}
8f=	273.55cm^{-1}	370.10cm^{-1}	340.49cm^{-1}	409.82cm^{-1}
9f=	243.84cm^{-1}	277.60cm^{-1}	245.76cm^{-1}	366.54cm^{-1}
10f=	195.76cm^{-1}	221.32cm^{-1}	166.83cm^{-1}	335.55cm^{-1}
11f=	155.51cm^{-1}	162.95cm^{-1}	141.65cm^{-1}	288.83cm^{-1}
12f=	43.61cm^{-1}	137.75cm^{-1}	75.43cm^{-1}	231.89cm^{-1}

Table S21. Catalytic performance of iron-based catalysts

Catalysts	Rate (CO_2) [moleculeCO_2/nm^2Fe/h]
Fe_3O_4	4.29
χ-Fe_5C_2	48.23
θ-Fe_3C	22.50

References

[1] G. Kresse, J. Hafner, Ab initio molecular dynamics for liquid metals, Phys. Rev. B 47 (1993) 558-561.

[2] G. Kresse, J. Hafner, Ab initio molecular-dynamics simulation of the liquid-metal--amorphous-semiconductor transition in germanium, Phys. Rev. B 49 (1994) 14251-14269.

[3] G. Kresse, J. Furthmüller, Efficient iterative schemes for ab initio total-energy calculations using a plane-wave basis set, Phys. Rev. B 54 (1996) 11169-11186.

[4] G. Kresse, J. Furthmüller, Efficiency of ab-initio total energy calculations for metals and semiconductors using a plane-wave basis set, Comput. Mater. Sci. 6 (1996) 15-50.

[5] P.E. Blöchl, Projector augmented-wave method, Phys. Rev. B 50 (1994) 17953-17979.

[6] J.P. Perdew, K. Burke, M. Ernzerhof, Generalized Gradient Approximation Made Simple, Phys. Rev. Lett. 77 (1996) 3865-3868.

[7] J.P. Perdew, J.A. Chevary, S.H. Vosko, K.A. Jackson, M.R. Pederson, D.J. Singh, C. Fiolhais, Atoms, molecules, solids, and surfaces: Applications of the generalized gradient approximation for exchange and correlation, Phys. Rev. B 46 (1992) 6671-6687.

[8] H.J. Monkhorst, J.D. Pack, Special points for Brillouin-zone integrations, Phys. Rev. B 13 (1976) 5188-5192.

[9] M. Methfessel, A.T. Paxton, High-precision sampling for Brillouin-zone integration in metals, Phys. Rev. B 40 (1989) 3616-3621.

[10] G. Henkelman, H. Jónsson, Improved tangent estimate in the nudged elastic band method for finding minimum energy paths and saddle points, J. Chem. Phys. 113 (2000) 9978-9985.

[11] G. Henkelman, H. Jónsson, A dimer method for finding saddle points on high dimensional potential surfaces using only first derivatives, J. Chem. Phys. 111 (1999) 7010-7022.

[12] G. Henkelman, A. Arnaldsson, H. Jónsson, A fast and robust algorithm for Bader decomposition of charge density, Comput. Mater. Sci. 36 (2006) 354-360.

[13] E. Sanville, D. Kenny Steven, R. Smith, G. Henkelman, Improved grid-based algorithm for Bader charge allocation, J. Comput. Chem. 28 (2007) 899-908.

[14] Y. Wang, Y. Li, S. Huang, J. Wang, H. Wang, J. Lv, X. Ma, Insight into CH4 formation and chain growth mechanism of Fischer−Tropsch synthesis on θ-Fe3C(031), Chem. Phys. Lett. 682 (2017) 115-121.

[15] T.H. Pham, X. Duan, G. Qian, X. Zhou, D. Chen, CO Activation Pathways of Fischer–Tropsch Synthesis on χ-Fe5C2 (510): Direct versus Hydrogen-Assisted CO Dissociation, J. Phys. Chem. C 118 (2014) 10170-10176.

[16] J.J. Retief, Powder diffraction data and Rietveld refinement of Hägg-carbide, χ-Fe5C2, Powder Diffr. 14 (1999) 130-132.

[17] S. Zhao, X.-W. Liu, C.-F. Huo, Y.-W. Li, J. Wang, H. Jiao, Surface morphology of Hägg iron carbide (χ-Fe5C2) from ab initio atomistic thermodynamics, J. Catal. 294 (2012) 47-53.

[18] D.C. Sorescu, Plane-Wave Density Functional Theory Investigations of the Adsorption and Activation of CO on Fe5C2 Surfaces, J. Phys. Chem. C 113 (2009) 9256-9274.

[19] E.J. Fasiska, G.A. Jeffrey, On the cementite structure, Acta Crystallogr. 19 (1965) 463-471.

[20] X.-Y. Liao, D.-B. Cao, S.-G. Wang, Z.-Y. Ma, Y.-W. Li, J. Wang, H. Jiao, Density functional theory study of CO adsorption on the (100), (001) and (010) surfaces of Fe3C, J. Mol. Catal. A: Chem. 269 (2007) 169-178.